RESEARCH ARTICLE

NANO · MICRO small
www.small-journal.com

Stability Enhancement in All-Inorganic Perovskite Light Emitting Diodes via Dual Encapsulation

Jindou Shi, Zeyu Wang, Nikolai V. Gaponenko, Zheyuan Da, Chen Zhang, Junnan Wang, Yongqiang Ji, Yusong Ding, Qing Yao, Youlong Xu, and Minqiang Wang*

Addressing the challenge of lighting stability in perovskite white light emitting diodes (WLEDs) is crucial for their commercial viability. $CsPbX_3$ (X = Cl, Br, I, or mixed) nanocrystals (NCs) are promising for next-generation lighting due to their superior optical and electronic properties. However, the inherent soft material structure of $CsPbX_3$ NCs is particularly susceptible to the elevated temperatures associated with prolonged WLED operation. Additionally, these NCs face stability challenges in high humidity environments, leading to reduced lighting performance. This study introduces a two-step dual encapsulation method, resulting in $CsPbBr_3$@SiO_2/Al_2SiO_5 composite fibers (CFs) with enhanced optical stability under extreme conditions. In testing, WLEDs incorporating these CFs, even under prolonged operation at high power (100 mA for 9 h), maintain consistent electroluminescence (EL) intensity and optoelectronic parameters, with surface temperatures reaching 84.2 °C. Crucially, when subjected to 85 °C and 85% relative humidity for 200 h, the WLEDs preserve 97% of their initial fluorescence efficiency. These findings underscore the efficacy of the dual encapsulation strategy in significantly improving perovskite material stability, marking a significant step toward their commercial application in optoelectronic lighting.

1. Introduction

Cesium lead halide perovskite $CsPbX_3$ (X = Cl, Br, I, or mixed) nanocrystals (NCs) are emerging as promising candidates for next-generation optical lighting materials, owing to their exceptional optoelectronic properties including high photoluminescence quantum yields (PLQYs), tunable band gaps, and narrow emission.[1–7] Despite these advantages, $CsPbX_3$ NCs are sensitive to environmental variations, particularly high temperatures, which even in minimal increments, can significantly deteriorate their optical properties.[8–11] Furthermore, exposure to environmental humidity can lead to partial decomposition of these NCs, negatively impacting fluorescence quality.[12,13] In optoelectronic devices, prolonged high-power operation generates high surface temperatures,[14–17] adversely affecting the optical characteristics of internal fluorescent materials. Therefore, enhancing the thermal stability of $CsPbX_3$ NCs is a critical and increasingly researched area in the field.[18,19]

Surface encapsulation with more stable materials has emerged as a prevalent approach for enhancing the stability of $CsPbX_3$ NCs. Various researchers have explored different encapsulation techniques to ensure the reliability of optoelectronic devices.[20–23] For instance, the use of thermoplastic polyurethane (TPU), a low-cost flexible polymer, as an encapsulation layer resulted in $CsPbBr_3$/TPU films with green fluorescence emission. This approach reduced the photoluminescence (PL) loss ratio to 47% under heating and cooling cycles at 363 K.[24] Similarly, encapsulating $CsPbBr_3$ NCs in dual-shell hollow SiO_2 spheres produced $CsPbBr_3$/SiO_2 nanospheres, which retained 65% of their PL intensity under a thermal environment at 100°C. The resulting white light emitting diode (WLED) devices achieved a wide color gamut, covering 136% of the NTSC standard.[25] Furthermore, $CsPbBr_3$@$CsPb_2Br_5$ core–shell microplates, created via a one-step encapsulation using $CsPbBr_3$ derivative $CsPb_2Br_5$, demonstrated a PL loss ratio of only 40% under similar thermal cycles and led to LED devices with a half-life of 19.4 h under high-power operation.[26] However, despite these advancements in thermal stability, the encapsulated $CsPbBr_3$ NCs have yet to achieve non-loss in PL intensity at high temperatures, which is a critical requirement for further commercial development. Consequently, achieving optimal optical stability of $CsPbBr_3$ NCs under high-temperature conditions remains a significant challenge.

J. Shi, Z. Da, C. Zhang, J. Wang, Y. Ji, Y. Ding, Q. Yao, Y. Xu, M. Wang
Electronic Materials Research Laboratory
Key Laboratory of the Ministry of Education International Center for Dielectric Research&Shannxi Engineering Research Center of Advanced Energy Materials and Devices
Xi'an Jiaotong University
Xi'an 710049, China

Z. Wang
Frontier Institute of Science and Technology (FIST)
Micro- and Nano-technology Research Center of State Key Laboratory for Manufacturing Systems Engineering
Xi'an Jiaotong University
Xi'an 710049, China
E-mail: zeyu.wang@xjtu.edu.cn

N. V. Gaponenko
Belarusian State University of Informatics and Radioelectronics
P. Browki 6, Minsk 220013, Belarus

The ORCID identification number(s) for the author(s) of this article can be found under https://doi.org/10.1002/smll.202310478

DOI: 10.1002/smll.202310478

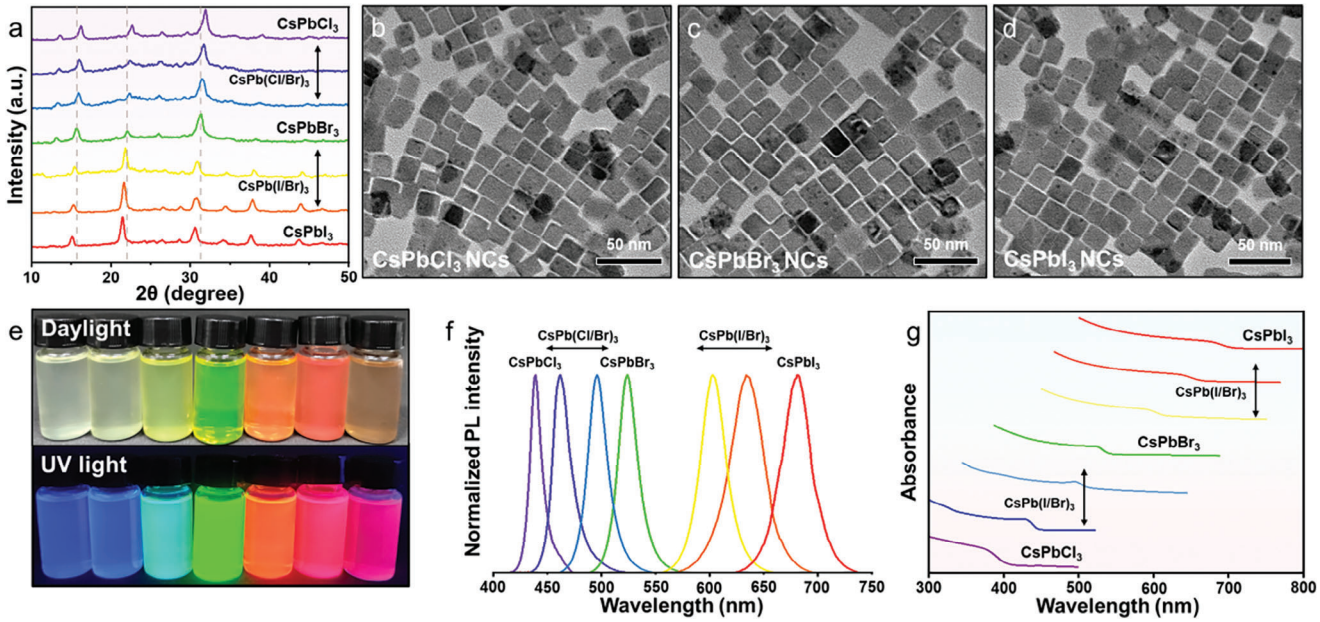

Figure 1. a) X-ray diffraction (XRD) patterns of $CsPbX_3$ (X = Cl, Br, I or mixed) NCs. Transmission electron microscope (TEM) images of b) $CsPbCl_3$ NCs, c) $CsPbBr_3$ NCs and d) $CsPbI_3$ NCs. Photographs e) of $CsPbX_3$ (X = Cl, Br, I or mixed) NCs under daylight (top) and UV light (bottom). Normalized photoluminescence (PL) f) and absorbance g) spectra of $CsPbX_3$ (X = Cl, Br, I or mixed) NCs.

In this study, a novel two-step encapsulation method was proposed to enhance the stability of $CsPbBr_3$ nanocrystals. Initially, a highly transmittable and water-resistant SiO_2 layer was applied as the primary encapsulation.[27,28] Subsequent encapsulation with high-temperature-resistant aluminosilicate composite fibers (Al_2SiO_5 CFs)[29,30] led to the creation of $CsPbBr_3@SiO_2/Al_2SiO_5$ CFs, exhibiting substantial thermal and water stability. As can be seen from further thermal, water and UV radiation stability tests, the optical properties of $CsPbBr_3@SiO_2/Al_2SiO_5$ CFs are not attenuated under high temperature (100°C), long-term water immersion (90 min) as well as UV irradiation (24 h), laying a solid foundation for subsequent applications in optoelectronic devices. Subsequently, the two-step encapsulation method was applied to obtain $CsPbI_3@SiO_2/Al_2SiO_5$ CFs and $CsPbCl_3@SiO_2/Al_2SiO_5$ CFs, respectively, and by adjusting the red, green, blue (RGB) ratio, the stable WLED device was assembled, which showed no significant variations in electroluminescence (EL) intensity as well as other optoelectronic parameters after 9 h of continuous working at high power (100 mA), although the surface temperature of the device was already as high as 84.2 °C at this time. Especially, the WLED was also exposed to more harsh environments (85 °C/85% relative humidity (RH)) for long-term stability tests, and its luminous efficiency was maintained at the initial 97% after 200 h of storage. This outstanding lighting stability perfectly meets the current market requirements for WLED devices, dramatically boosting the competitiveness of perovskite materials for the commercial lighting sector in the future.

2. Results and Discussion

$CsPbX_3$ (X = Cl, Br, I or mixed) NCs with different halide ion contents were obtained by conventional high-temperature thermal injection (specific preparation in Supporting Information). The XRD pattern revealed that all samples matched the typical cubic phase, and as the X-site ions were transitioned from Cl^- to I^-, the corresponding diffraction peaks were shifted toward a smaller 2θ angles (**Figure 1a**), which was attributed to the lattice expansion induced by the increased radius of the halide ion (Cl^-: 167 pm, Br^-: 182 pm, I^-: 206 pm).[31,32] All samples presented a typical neat cubic arrangement (Figure 1b–d), indicating excellent mono-dispersibility, which was consistent with that previously reported.[33] $CsPbX_3$ (X = Cl, Br, I, or mixed) NCs exhibited bright fluorescence emission with various colors under UV light irradiation (Figure 1e), corresponding to PL spectra covering the whole visible region (Figure 1f). Such optical behaviors resulted mainly from the gradual transfer of the halide ions from Cl^- to I^-, causing a shifting in the absorption edge of $CsPbX_3$ NCs (Figure 1g). In summary, the whole spectral emission of $CsPbX_3$ NCs in the visible region can be achieved by simply adjusting the ratio of halide ions, as well as their low production cost making them the most promising material for optical illumination.

Unfortunately, commercial lighting devices inevitably generate high temperatures on the surface of the backlight chips under prolonged energization, which can be fatal to the optical properties of the fluorescent material, so that improving the optical stability of commercial lighting phosphors under thermal environments has been the bottleneck in their development for a long time.[34,35] Particularly, cesium lead halide perovskite $CsPbX_3$ NCs belong to a soft matter system in structure, which will display a large response to minor changes in the external thermal environment,[36] accompanied by a degradation of their optical properties, greatly limiting their application in the field of commercial lighting. Moreover, some lighting devices in practical applications will be exposed to high humidity environments for long periods of time, and the ionic

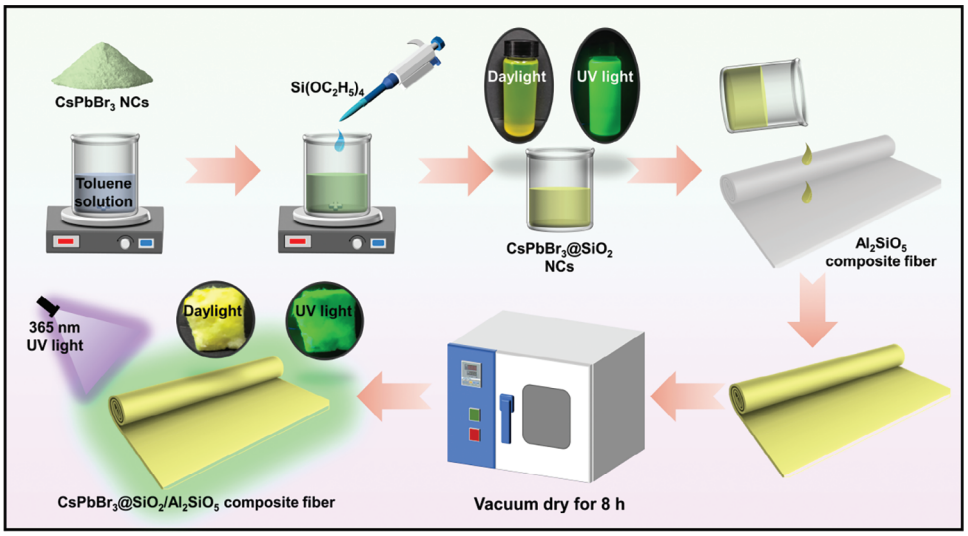

Figure 2. Schematic diagram of the highly stable $CsPbBr_3@SiO_2/Al_2SiO_5$ CFs were obtained by dual encapsulation treatment for $CsPbBr_3$ NCs.

nature of CsPbX3 NCs themselves makes them susceptible to moisture-induced decomposition,[37] so addressing their optical stability under high-humidity environments will contribute to their sustainable development. Here, it is proposed to accomplish the thermal stability enhancement of $CsPbX_3$ NCs by applying a two-step dual encapsulation strategy (**Figure 2**), where $CsPbBr_3$ NCs will be selected as the object of study. First, $CsPbBr_3$ NCs were dispersed in a toluene solution and encapsulated with a highly transmissive layer of SiO_2 by the hydrolysis process of $Si(OC_2H_5)_4$, thereby effectively enhancing the water stability of $CsPbBr_3$ NCs and partially improving their thermal stability. Subsequently, the obtained $CsPbBr_3@SiO_2$ core-shell NCs were composited with the thermostable Al_2SiO_5 CFs to produce $CsPbBr_3@SiO_2/Al_2SiO_5$ CFs with excellent thermal stability, which exhibited bright green fluorescence emission under UV light irradiation, so that the two-step dual encapsulation strategy would not affect the optical properties of $CsPbBr_3$ NCs.

The microstructure and morphology of the samples under each encapsulation step were closely observed respectively, thereby providing an insight into the preparation process. The thermal injection method produced cubic $CsPbBr_3$ NCs with excellent crystallinity (**Figure** 3a), where the lattice spacing of 0.41 nm corresponded exactly to the (114) crystal plane (Figure 3b). Moreover, elemental mapping and energy dispersive spectroscopy (EDS) results (Figure S1, Supporting Information) showed that Cs, Pb, and Br were uniformly distributed in the crystal with no additional elements, which again ensured the synthesis of high-quality $CsPbBr_3$ NCs. After being encapsulated with SiO_2, it can be seen that core $CsPbBr_3$ NCs no longer retained the initial cubic shape (Figure 3c), resulting from the erosion of the surface of $CsPbBr_3$ NCs during the hydrolysis of $Si(OC_2H_5)_4$, a similar phenomenon was reported in the previous preparation of $CsPbBr_3@ZrO_2$ NCs.[38] In the HR-TEM image of $CsPbBr_3@SiO_2$ NCs (Figure 3d), the lattice spacing of the internal $CsPbBr_3$ NCs can be clearly seen, corresponding exactly to the crystal plane of $CsPbBr_3$. Additionally, an encapsulated layer of amorphous SiO_2 can also be observed on the surface of $CsPbBr_3$ NCs, therefore showing no obvious lattice. Subsequently, elemental mapping and EDS results of $CsPbBr_3@SiO_2$ NCs demonstrated that Si and O elements were detected on the surface of $CsPbBr_3$ NCs (Figure S2, Supporting Information), indicating that the first encapsulation of $CsPbBr_3$ NCs was successfully completed using the hydrolysis of $Si(OC_2H_5)_4$. Subsequently, the secondary encapsulation was completed by compositing $CsPbBr_3@SiO_2$ NCs with the high-temperature resistant Al_2SiO_5 CFs. Notably, a smooth surface of the pure phase Al_2SiO_5 CFs was observed, which intertwined together to form large filling spaces, thereby facilitating a better entry of $CsPbBr_3@SiO_2$ NCs (Figure S3, Supporting Information). $CsPbBr_3@SiO_2/Al_2SiO_5$ CFs were acquired after compositing $CsPbBr_3@SiO_2$ NCs into Al_2SiO_5 CFs, the corresponding SEM image revealed that the surface of Al_2SiO_5 CFs was no longer smooth (Figure 3e), and a large amount of $CsPbBr_3@SiO_2$ NCs could be seen attached to each Al_2SiO_5 fiber on the HR-SEM image (Figure 3f). Afterward, the compositing of $CsPbBr_3@SiO_2$ NCs in Al_2SiO_5 CFs was analyzed by elemental mapping and EDS (Figure S4, Supporting Information), which indicated that the elements of Al_2SiO_5 CFs were distributed along the fiber orientation, the elements of $CsPbBr_3@SiO_2$ NCs were uniformly distributed on their surface, and all elemental signals have been detected. Moreover, the diffraction peaks of $CsPbBr_3$ were detected in the XRD patterns of all samples (Figure 3g), indicating that the dual encapsulation strategy did not have a significant impact on the crystal structure of $CsPbBr_3$ NCs. The above characterization results indicated that $CsPbBr_3@SiO_2/Al_2SiO_5$ CFs were successfully prepared by utilizing a convenient two-step dual encapsulation strategy, which laid the foundation for subsequent optical development.

In order to better understand the effect of the dual encapsulation strategy on the fluorescence emission of $CsPbBr_3$ NCs, the changing optical properties of the samples before and after encapsulation were investigated closely. The fluorescence emission peaks of all samples were located in the green region, with the slight distinction that the PL emission peaks of $CsPbBr_3@SiO_2$ NCs (518 nm) and $CsPbBr_3@SiO_2/Al_2SiO_5$ CFs (518 nm) showed a small blue shift in position relative

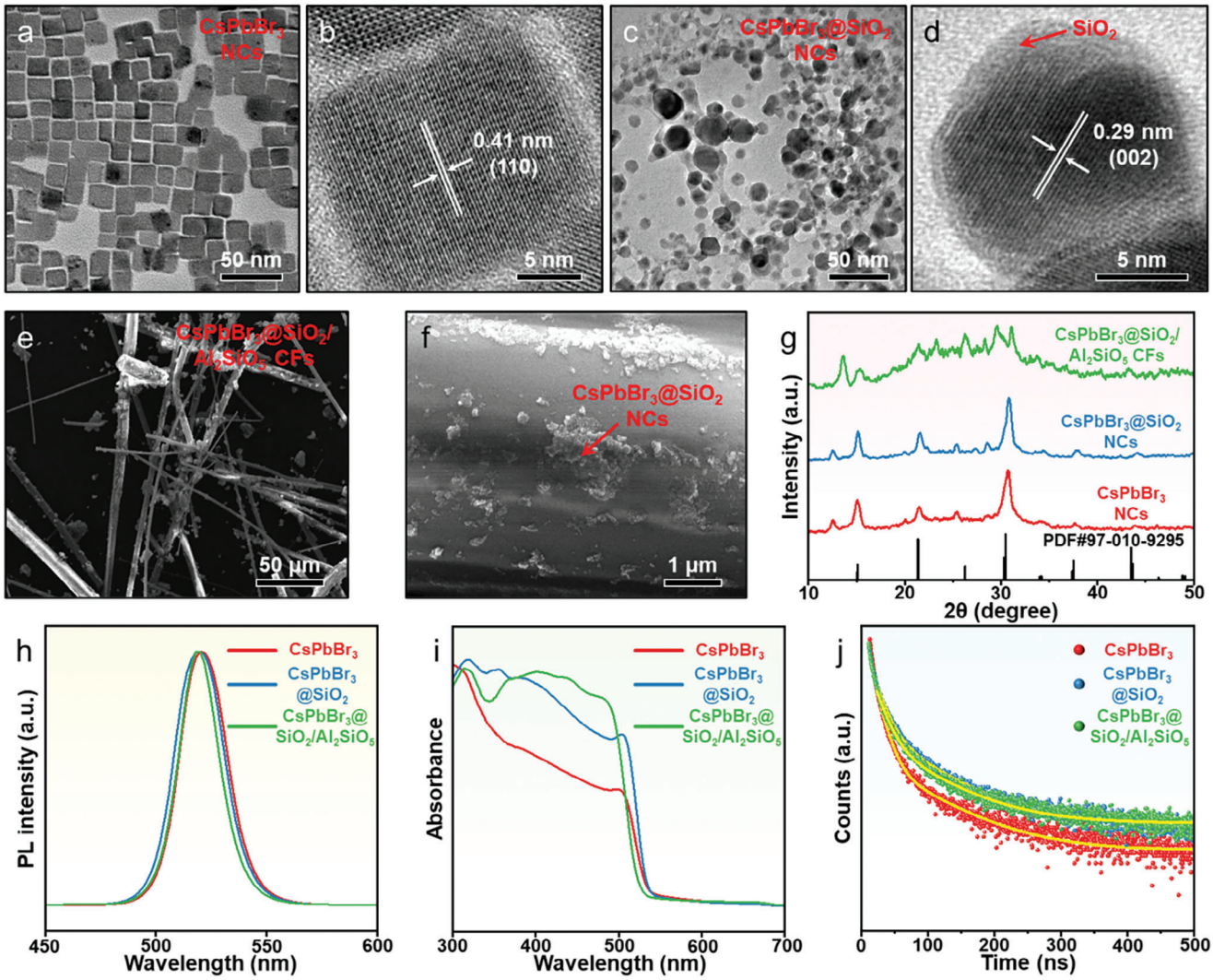

Figure 3. TEM and high-resolution transmission electron microscope (HR-TEM) images of a,b) $CsPbBr_3$ NCs and c,d) $CsPbBr_3@SiO_2$ NCs. Scanning electron microscope (SEM) and high-resolution scanning electron microscope (HR-SEM) images of e,f) $CsPbBr_3@SiO_2/Al_2SiO_5$ CFs. g) XRD patterns of $CsPbBr_3$ NCs (red), $CsPbBr_3@SiO_2$ NCs (blue) and $CsPbBr_3@SiO_2/Al_2SiO_5$ CFs (green). h) Normalized PL, i) absorbance, and j) time-resolved PL spectra of samples.

to $CsPbBr_3$ NCs (522 nm) (Figure 3h). This mainly stemmed from the size shrinkage caused by the corrosion of core $CsPbBr_3$ NCs during hydrolysis, which triggered a blue shift in the PL emission peak.[39] The PLQYs of $CsPbBr_3$ NCs (76%) after dual encapsulation were increased to 84% ($CsPbBr_3@SiO_2$ NCs) and 87% ($CsPbBr_3@SiO_2/Al_2SiO_5$ CFs) respectively, which can be explained by the passivation of their surface defects with SiO_2, a similar phenomenon having been observed in previous reports.[40] As can be seen from the corresponding absorbance spectra of the samples, the single or dual encapsulation did not impact on the absorbance of $CsPbBr_3$ NCs, and their absorption edges remained the same (Figure 3i), which again demonstrated that the dual encapsulation strategy only enhanced their stability and not interfered with the crucial optical properties. Finally, the carrier recombination dynamics of the samples were investigated by recording the change in PL lifetime decay behaviors before and after encapsulation (Figure 3j). The results indicated that the PL decay curves of the samples were well fitted by the dual exponential decay function (Table S1, Supporting Information), where the short lifetime (τ_1) was derived from the non-radiative recombination and the long lifetime (τ_2) was attributed to the radiative recombination.[41,42] The radiative recombination ratio (A_2) of samples after encapsulation was improved, indicating that the internal defect state content was reduced, which coincided with the increasing trend of their PLQYs. By comparing the optical behaviors before and after encapsulation, it can be concluded that the dual encapsulation strategy not only did not hinder the fluorescence emission of $CsPbBr_3$ NCs, but rather acted as a facilitator, which will pave the way for its application in the field of optoelectronic lighting.

Next, the optical properties of $CsPbBr_3$ NCs, $CsPbBr_3@SiO_2$ NCs, and $CsPbBr_3@SiO_2/Al_2SiO_5$ CFs were in situ observed under different thermal environments in order to better evaluate

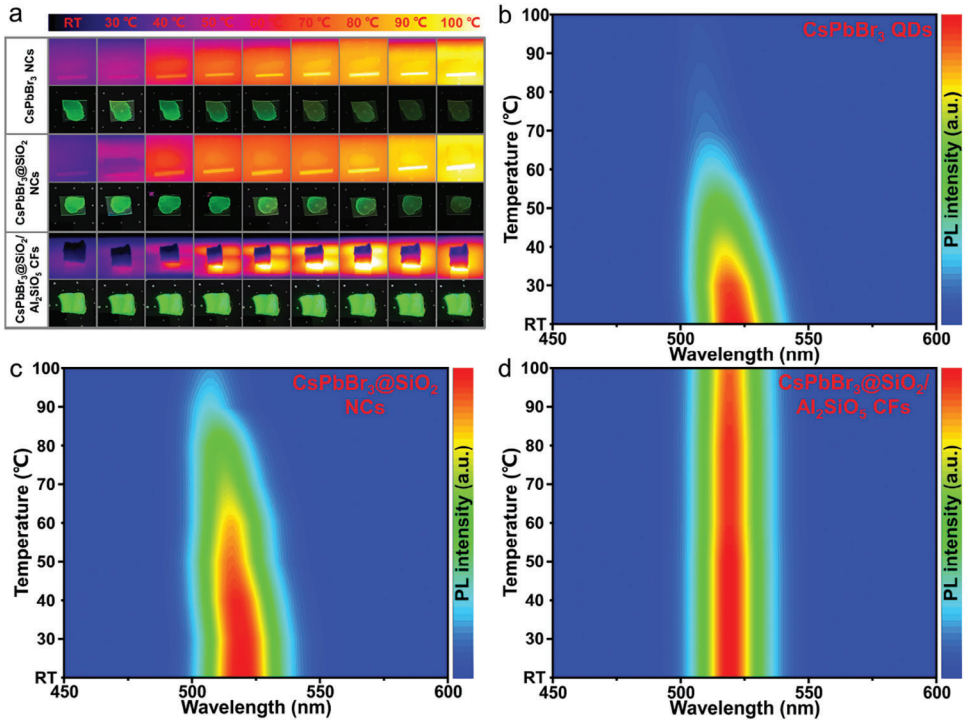

Figure 4. a) Infrared images and fluorescence photographs of $CsPbBr_3$ NCs, $CsPbBr_3@SiO_2$ NCs, and $CsPbBr_3@SiO_2/Al_2SiO_5$ CFs under different temperature were recorded by infrared thermal camera and photo camera, respectively. Changes in the instantaneous PL spectra of b) $CsPbBr_3$ NCs, c) $CsPbBr_3@SiO_2$ NCs, and d) $CsPbBr_3@SiO_2/Al_2SiO_5$ CFs from RT to 100 °C.

the improved thermal stability of the samples before and after encapsulation. Infrared images of $CsPbBr_3$ NCs, $CsPbBr_3@SiO_2$ NCs, and $CsPbBr_3@SiO_2/Al_2SiO_5$ CFs at different temperatures were recorded using a thermal infrared imager (**Figure 4a**). As can be seen the surface temperature of the unencapsulated $CsPbBr_3$ NCs and single encapsulated $CsPbBr_3@SiO_2$ NCs are consistent with the environmental temperature owing to the lack of a more thermo-resistant encapsulation layer, which directly resulted in the core light emitting layer ($CsPbBr_3$) being exposed to high-temperature environments, thereby brought about a greater threat to their optical stability. In stark contrast, after being encapsulated in Al_2SiO_5 CFs with excellent thermal insulation, the temperature on the surface of $CsPbBr_3@SiO_2/Al_2SiO_5$ CFs was only 30 °C when the external environmental temperature reached 100°C, greatly alleviating the effect of the thermal environment on its optical stability. Fluorescence photographs corresponding to the samples under UV light also demonstrated that the fluorescence emission of $CsPbBr_3@SiO_2/Al_2SiO_5$ CFs after dual encapsulation did not decay under high-temperature environments (100 °C), and the excellent optical stability will allow it to take advantage in the next step of lighting development. Subsequently, the PL spectra of $CsPbBr_3$ NCs, $CsPbBr_3@SiO_2$ NCs, and $CsPbBr_3@SiO_2/Al_2SiO_5$ CFs were in situ recorded at different temperatures to provide more insight into the effect of the thermal environment on the optical properties. Undoubtedly, there was a decrease in PL intensity for both $CsPbBr_3$ NCs and $CsPbBr_3@SiO_2$ NCs (Figure 4b,c), which corresponded to the fluorescence photographs at different temperatures (Figure 4a). However, the PL intensity decay of $CsPbBr_3@SiO_2$ NCs was alleviated compared to $CsPbBr_3$ NCs, which was mainly due to the encapsulation of the SiO_2 shell on its surface, suggesting that SiO_2 was also effective to improving the thermal stability of $CsPbBr_3$ NCs. Moreover, the PL emission peaks of both $CsPbBr_3$ NCs and $CsPbBr_3@SiO_2$ NCs displayed blue shift in different degree, which was caused by the out-of-phase band-edge states stabilized as lattice dilation at the Brillouin zone boundary, as mentioned in previous reports on the thermal stability of halide perovskite materials.[43–45] The most outstanding performance was in $CsPbBr_3@SiO_2/Al_2SiO_5$ CFs after dual encapsulation, which benefited from the protection of the SiO_2 and Al_2SiO_5 shell layers, allowing the environmental temperature of the core light-emitting layer ($CsPbBr_3$) to be kept at 30°C, so that its PL intensity did not show any significant decay and the position of the emission peak did not shift (Figure 4d). Afterward, heating-cooling cycles tests at high temperature (100 °C) were carried to $CsPbBr_3$ NCs, $CsPbBr_3@SiO_2$ NCs, and $CsPbBr_3@SiO_2/Al_2SiO_5$ CFs, and the PL intensity of the samples after each cycle was recorded respectively (Figure S5, Supporting Information). The results indicated that the double layer protected $CsPbBr_3@SiO_2/Al_2SiO_5$ CFs had excellent PL cycling stability, and the PL intensity was basically maintained in the initial state after ten sets of heating and cooling cycles, while both $CsPbBr_3$ NCs and $CsPbBr_3@SiO_2$ NCs suffered from severe fluorescence loss. Comparison of the optical stability of $CsPbBr_3$ NCs, $CsPbBr_3@SiO_2$ NCs, and $CsPbBr_3@SiO_2/Al_2SiO_5$ CFs demonstrated that $CsPbBr_3@SiO_2/Al_2SiO_5$ CFs was able to maintain stable fluorescence emission under high-temperature environment, which was crucial for the assembly of

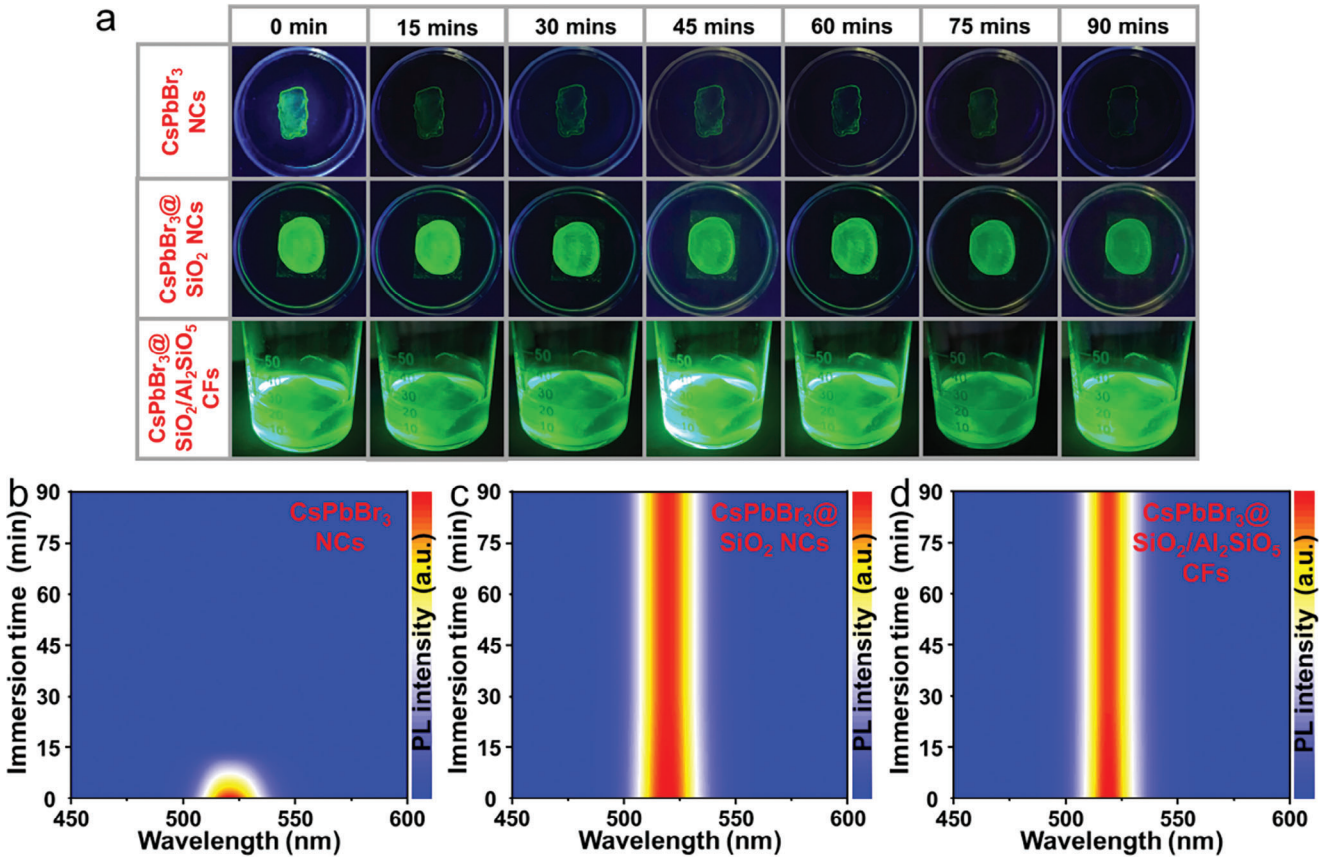

Figure 5. a) Fluorescence photographs of $CsPbBr_3$ NCs, $CsPbBr_3@SiO_2$ NCs and $CsPbBr_3@SiO_2/Al_2SiO_5$ CFs stored in water for different times. Changes in the instantaneous PL spectra of b) $CsPbBr_3$ NCs, c) $CsPbBr_3@SiO_2$ NCs, and d) $CsPbBr_3@SiO_2/Al_2SiO_5$ CFs stored in water from 0 min to 90 mins.

optoelectronic devices, as the devices would inevitably generate heat on the surface under long-term energized conditions, and the excellent thermal stability would greatly boost the competitiveness of $CsPbBr_3@SiO_2/Al_2SiO_5$ CFs in the field of lighting materials.

Subsequently, the long-term stability of $CsPbBr_3$ NCs, $CsPbBr_3@SiO_2$ NCs, and $CsPbBr_3@SiO_2/Al_2SiO_5$ CFs in water was further investigated to understand the impact of external environmental humidity on their optical properties. The samples were stored individually in water and the changes in their PL spectra at different times were recorded. It is evident that the fluorescence emission of $CsPbBr_3$ NCs rapidly deteriorated after being stored in water for 15 min (**Figure** 5a,b), mainly from the fact that direct exposure to large volumes of water caused the decomposition of the $CsPbBr_3$ NCs, thereby leading to a loss of optical properties. On the other hand, after being encapsulated by SiO_2, both $CsPbBr_3@SiO_2$ NCs (Figure 5a,c) and $CsPbBr_3@SiO_2/Al_2SiO_5$ CFs (Figure 5a,d) exhibited excellent optical stability in water, which was primarily attributed to the fact that the amorphous SiO_2 effectively constructed a barrier between the water molecules and $CsPbBr_3$ NCs, thus ensuring that the crystals did not decompose. In summary, the dual encapsulation strategy not only conferred excellent thermal stability to $CsPbBr_3$ NCs, but also enhanced its optical stability under high humidity environments, which further promoted the application of perovskite optical lighting devices in a variety of harsh environments.

Furthermore, UV irradiation stability also hindered the development of perovskite optoelectronic devices for a long time. Prolonged exposure to UV irradiation for $CsPbX_3$ NCs will produce halogen vacancy-halogen interstitial pairs, allowing the halogen to migrate to the perovskite surface, which can then be trapped by the ionic surface, leading to ligand desorption and crystal regeneration.[46,47] Many strategies have been proposed to overcome this defect, where encapsulation can effectively protect the bonded ligands on the surface of $CsPbX_3$ NCs, avoiding the formation of emission or no-emission traps, and preventing photo-induced regeneration and luminescence degradation of perovskite crystals.[48,49] Here, $CsPbBr_3$ NCs, $CsPbBr_3@SiO_2$ NCs, and $CsPbBr_3@SiO_2/Al_2SiO_5$ CFs were treated with UV irradiation for up to 24 h. It can be seen that both single-encapsulated $CsPbBr_3@SiO_2$ NCs and double-encapsulated $CsPbBr_3@SiO_2/Al_2SiO_5$ CFs exhibited excellent fluorescence stability (Figure S6a, Supporting Information). After long-term irradiation, they still maintained bright emission, which again proved the effectiveness of the encapsulation strategy, and laid the foundation for the subsequent assembly of highly stable perovskite LED devices.

For assessing the performance enhancement of perovskite optoelectronic lighting devices with the dual encapsulation strategy,

$CsPbCl_3$ NCs/$CsPbCl_3$@SiO_2 NCs/$CsPbCl_3$@SiO_2/Al_2SiO_5 CFs and $CsPbI_3$ NCs/$CsPbI_3$@SiO_2 NCs/$CsPbI_3$@SiO_2/Al_2SiO_5 CFs were obtained using the same encapsulation method and were applied as blue- and red-light sources, and three WLED devices were subsequently assembled by adjusting the ratio of the RGB. For easy labeling, the three types of WLED are still denoted as $CsPbBr_3$ NCs, $CsPbBr_3$@SiO_2 NCs, and $CsPbBr_3$@SiO_2/Al_2SiO_5 CFs representing unencapsulated, single encapsulated and dual encapsulated respectively. The EL intensity of the three WLED devices progressively intensified with increasing drive current (from 5 to 100 mA), and no significant apparent saturation was observed (Figure S7a–c, Supporting Information), implying that the WLEDs assembled with the three different materials were suitable for high-power commercial lighting systems. Furthermore, the corresponding correlated color temperature (CCT) and color rendering index (CRI) also gradually enhanced (Figure S7d–f, Supporting Information), with the CCT of the WLEDs assembled with $CsPbBr_3$ NCs, $CsPbBr_3$@SiO_2 NCs and $CsPbBr_3$@SiO_2/Al_2SiO_5 CFs reaching 10 344, 11 029, and 10 494 K respectively, and the CRI reaching 73, 87, and 85 respectively, when the drive current was 100 mA. At the same time, both three WLEDs are emitting bright white light (insets in Figure S7g–i, Supporting Information), corresponding to the color coordinates in the International Commission on Illumination (CIE) diagrams at (0.28, 0.29), (0.27, 0.30), and (0.29, 0.28) (Figure S7g–i, Supporting Information), which belong to the standard white light region, indicating that they can be applied as excellent lighting devices.

Importantly, the UV chip in the WLED inevitably generated high temperatures on its surface during long-term working, which had a fatal impact on the light-emitting layer. Therefore, the surface temperature and related optoelectronic parameters of the WLED device as function of working time were recorded by using thermal infrared imager and spectrometer respectively (**Figure 6**a). The surface temperature of WLED devices gradually increased with working time when operating at 100 mA high power, and the surface temperature of WLED devices was already up to 84.2 °C after working for 9 h (Figure 6b). There is no doubt that the EL intensity of the WLED devices assembled by $CsPbBr_3$ NCs and $CsPbBr_3$@SiO_2 NCs gradually reduced as the working time extended (Figure 6c,d). The relative humidity of the testing environment at this time was only 30%, so the effect of environmental humidity on EL intensity was ignored. Subsequently, the decay trends of RGB intensity in the WLED devices were collected respectively, and it can be seen that the decay trends of the three light sources were inconsistent, where the fastest decay in the red-light source (Figure S8a,b, Supporting Information), which made it impossible to guarantee the RGB ratio of the white light source, thereby unable to achieve a continuous output of white light. Meanwhile, the optoelectronic parameters of the WLED devices also showed dramatic variations, with the $CsPbBr_3$ NCs-assembled WLED devices exhibiting the most significant decay in luminous efficiency and wide fluctuation in CCT (Figure 6f). Benefiting from the SiO_2 protection layer, the variations in the optoelectronic parameters of the $CsPbBr_3$@SiO_2 NCs-assembled WLEDs were alleviated, but it cannot be stabilized either (Figure 6g), making it impossible to meet the demand for commercial lighting. Contrastingly, the $CsPbBr_3$@SiO_2/Al_2SiO_5 CFs-assembled WLED device displayed excellent lighting stability (Figure 6e), with the dual-layer encapsulation allowing its RGB intensity to be essentially unchanged, maintaining a stable white light output. Corresponding optoelectronic parameters were very stable, the luminous efficiency of the device being maintained ≈32 lm W^{-1}, and the CCT being stabilized at ≈10 000 K (Figure 6h), which again suggested that after the dual encapsulation, $CsPbBr_3$@SiO_2/Al_2SiO_5 CFs had overcome the thermal effect on the surface of the optoelectronic device, thereby ensuring an efficient white light output. Subsequently, the operational stability of the WLED was recorded by exposing it under 85 °C and 85% RH (Figure S9a, Supporting Information), thereby ensuring that it could be adapted to a variety of extreme practical application environments. The luminous efficiency of the WLED device was 31.2 lm W^{-1} after being stored in a harsh environment for 200 h (Figure S9b, Supporting Information), which was ≈97% of the initial intensity (32 lm W^{-1}). Compared with the perovskite LED devices obtained from other stability enhancement strategies (Table S2, Supporting Information), the device performance obtained from this dual-encapsulation treatment was most outstanding, and the device lifetime was greatly extended, which will provide a new option for subsequent commercial development. From the above practical optoelectronic applications, the $CsPbX_3$@SiO_2/Al_2SiO_5 (X = Cl, Br, I) CFs obtained from the dual encapsulation strategy have been the perfect choice for assembling perovskite lighting devices, and the excellent long-term working stability under high power will bring a new gospel for efficient and stable perovskite WLED devices.

3. Conclusion

In summary, this study presents a straightforward two-step dual encapsulation strategy, employing highly transmittable and water-stable SiO_2 along with high-temperature-resistant Al2SiO5 composite fibers (CFs) as encapsulation layers, to achieve highly stable $CsPbBr_3$@SiO_2/Al_2SiO_5 CFs. Subsequently, the optical stability of unencapsulated $CsPbBr_3$ NCs, single encapsulated $CsPbBr_3$@SiO_2 NCs and dual encapsulated $CsPbBr_3$@SiO_2/Al_2SiO_5 CFs was compared under high temperature, long-term water immersion as well as UV irradiation, and the results showed that $CsPbBr_3$@SiO_2/Al_2SiO_5 CFs after dual encapsulation exhibited excellent thermal, water and UV irradiation stability. Conversely, employing the dual encapsulation strategy yielded $CsPbCl_3$@SiO_2/Al_2SiO_5 CFs and $CsPbI_3$@SiO_2/Al_2SiO_5 CFs. A WLED device, demonstrating a luminous efficiency of 32 lm W^{-1}, was assembled by finely tuning the RGB ratio. Operated at a high power of 100 mA for 9 h, the device maintained stable electroluminescence (EL) intensity, and other related optoelectronic parameters remained constant. Notably, the surface temperature of the device reached 84.2 °C, as detected by a thermal infrared imager, without significantly impacting performance. Moreover, the WLED was exposed to a harsh environment of 85 °C/85%RH for long-term stability testing, and its luminous efficiency was maintained at the initial 97% after being stored for 200 h. We believe that this two-step dual encapsulation strategy could significantly facilitate the development of highly stable WLED devices, consequently expanding the scope of commercial applications for perovskite materials.

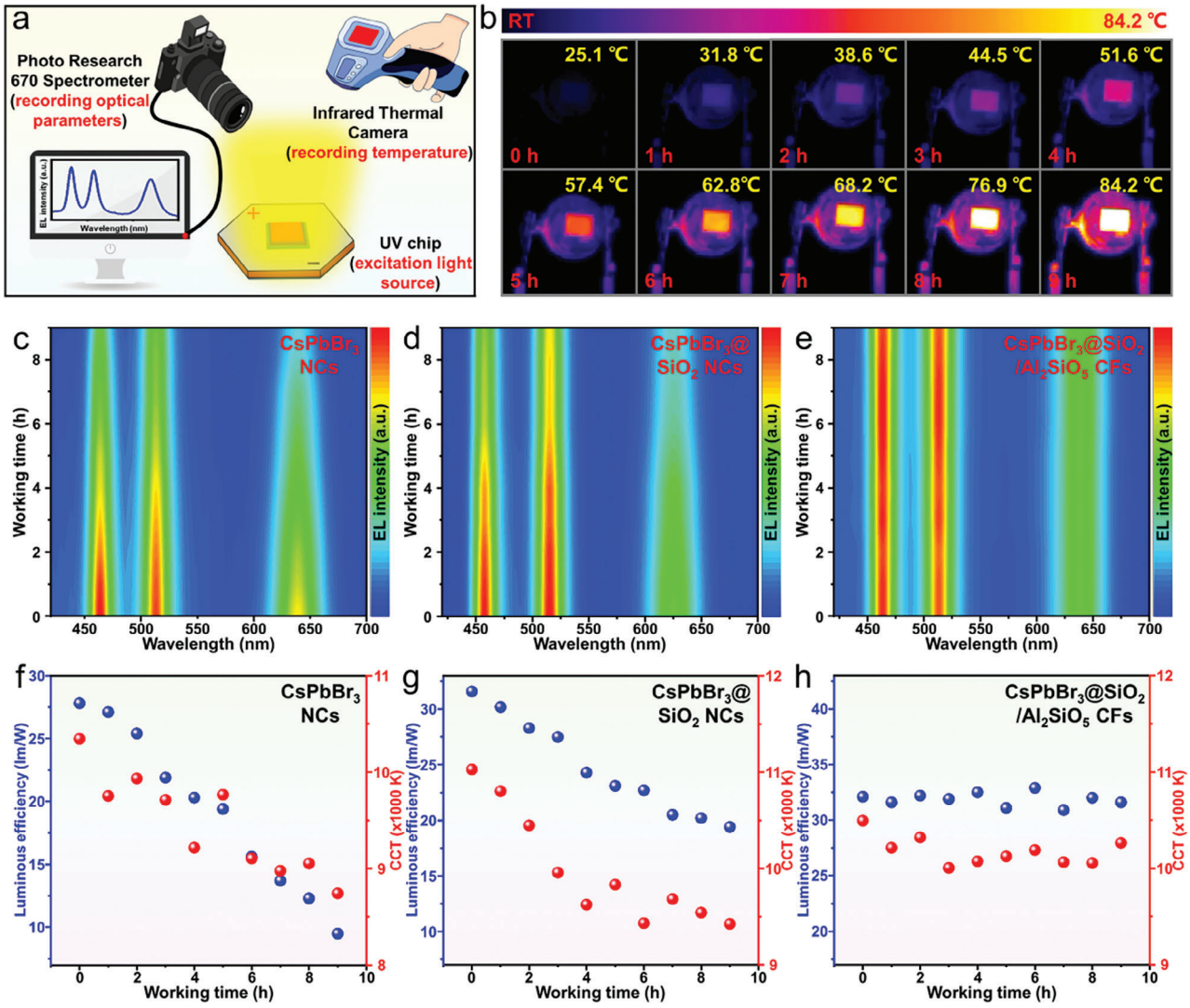

Figure 6. a) Schematic of WLED devices surface temperature and EL spectra collection during operation. Infrared images and surface temperature b) of WLED devices driven by 100 mA current with extended working time. Changes in the EL spectra, luminous efficiency (blue dot), and CCT (red dot) of the WLEDs assembled by c,f) $CsPbBr_3$ NCs, d,g) $CsPbBr_3@SiO_2$ NCs and e,h) $CsPbBr_3@SiO_2/Al_2SiO_5$ CFs with extended working time.

Supporting Information

Supporting Information is available from the Wiley Online Library or from the author.

Acknowledgements

This work was supported by the National Key Research and Development Program of China (2022YFE0122500 and 2019YFB1503200), the National Natural Science Foundation of China (NSFC, 52161145103 and 61774124), 111 Program (No. B14040), and Shaanxi Provincial Key Research and Development Program (No. 2021GXLH-Z-084). The authors thank Ms. Dan He at Instrument Anaysis Center of Xi'an Jiaotong University for her help with the time-resolved PL analysis.

Conflict of Interest

The authors declare no conflict of interest.

Data Availability Statement

Research data are not shared.

Keywords

$CsPbBr_3$ NCs, $CsPbX_3@SiO_2/Al_2SiO_5$ CFs, dual encapsulation, thermal stability, white light emitting diode

Received: November 15, 2023
Revised: January 19, 2024
Published online: February 9, 2024

[1] T. J. Milstein, D. M. Kroupa, D. R. Gamelin, *Nano Lett.* **2018**, *18*, 3792.
[2] A. Dutta, R. K. Behera, P. Pal, S. Baitalik, N. Pradhan, *Angew. Chem., Int. Ed.* **2019**, *58*, 5552.

[3] J. D. Lin, Y. X. Lu, X. Y. Li, F. Huang, C. B. Yang, M. L. Liu, N. Z. Jiang, D. Q. Chen, *ACS Energy Lett.* **2021**, *6*, 519.
[4] Y. F. Yue, D. X. Zhu, N. Zhang, G. S. Zhu, Z. M. Su, *ACS Appl. Mater. Interfaces* **2019**, *11*, 15898.
[5] C. Otero-Martinez, M. Imran, N. J. Schrenker, J. Z. Ye, K. Y. Ji, A. Rao, S. D. Stranks, R. L. Z. Hoye, S. Bals, L. Manna, J. Perez-Juste, L. Polavarapu, *Angew. Chem., Int. Ed.* **2022**, *61*, 2205617.
[6] S. X. Li, Y. Pan, W. M. Wang, Y. Li, *Chem. Eng. J.* **2022**, *434*, 134593.
[7] S. X. Liao, Z. Z. Yang, J. D. Lin, S. X. Wang, J. W. Zhu, S. X. Chen, F. Huang, Y. H. Zheng, D. Q. Chen, *Adv. Funct. Mater.* **2023**, *33*, 2210558.
[8] G. Z. Li, Q. W. Pan, Z. H. Zhou, R. R. Gu, H. Zhang, X. J. Huang, G. P. Dong, X. D. Xiao, *Adv. Opt. Mater.* **2023**, *11*, 2203028.
[9] J. J. Ren, A. Meijerink, X. P. Zhou, J. P. Wu, G. Y. Zhang, Y. H. Wang, *ACS Appl. Mater. Interfaces* **2022**, *14*, 3176.
[10] H. B. Chen, Y. J. Ma, X. P. Wang, G. W. Yao, Y. C. Du, J. Y. Zhou, L. Z. Zhu, X. H. Zhao, S. P. Yang, X. P. Liu, M. L. Cai, S. Y. Dai, *Chem. Eng. J.* **2022**, *442*, 136242.
[11] W. C. Chen, L. C. Chen, F. J. Liu, W. C. Tsai, B. H. Tung, M. Venkatesan, M. L. Tsai, J. H. Lin, C. C. Kuo, *Small* **2023**, *19*, 2207685.
[12] S. Song, Y. C. Lv, B. Q. Cao, W. Z. Wang, *Adv. Funct. Mater.* **2023**, *33*, 2300493.
[13] Q. X. Zhong, X. C. Wang, M. Y. Chu, Y. H. Qiu, D. Yang, T. K. Sham, J. X. Chen, L. Wang, M. H. Cao, Q. Zhang, *Small* **2022**, *18*, 2107548.
[14] J. H. Ji, G. Jo, J. G. Ha, S. M. Koo, M. Kamiko, J. Hong, J. H. Koh, *J Nanosci Nanotechnol* **2018**, *18*, 6029.
[15] Z. Sun, D. M. Wu, Y. J. Zhang, J. Zhuang, K. F. Deng, *Key Eng. Mater.* **2012**, *503*, 397.
[16] X. Y. Lu, T. C. Hua, Y. P. Wang, *Microelectron. J.* **2011**, *42*, 1257.
[17] M. M. Liu, Q. Wan, H. M. Wang, F. Carulli, X. C. Sun, W. L. Zheng, L. Kong, Q. Zhang, C. Y. Zhang, Q. G. Zhang, S. Brovelli, L. Li, *Nat. Photonics* **2021**, *15*, 379.
[18] X. L. Dai, Y. Z. Deng, X. G. Peng, Y. Z. Jin, *Adv. Mater.* **2017**, *29*, 1607022.
[19] R. J. Sutton, G. E. Eperon, L. Miranda, E. S. Parrott, B. A. Kamino, J. B. Patel, M. T. Horantner, M. B. Johnston, A. A. Haghighirad, D. T. Moore, H. J. Snaith, *Adv. Energy Mater.* **2016**, *6*, 1502458.
[20] W. Z. Lv, L. Li, M. C. Xu, J. X. Hong, X. X. Tang, L. G. Xu, Y. H. Wu, R. Zhu, R. F. Chen, W. Huang, *Adv. Mater.* **2019**, *31*, 1502458.
[21] Y. Q. Ji, M. Q. Wang, Z. Yang, H. Wang, M. A. Padhiar, J. D. Shi, H. W. Qu, A. S. Bhatti, *J. Phys. Chem. C* **2022**, *126*, 1542.
[22] Q. G. Zhang, B. Wang, W. L. Zheng, L. Kong, Q. Wan, C. Y. Zhang, Z. C. Li, X. Y. Cao, M. M. Liu, L. Li, *Nat. Commun.* **2020**, *11*, 31.
[23] A. Z. Pan, M. J. Jurow, F. Qiu, J. Yang, B. Y. Ren, J. J. Urban, L. He, Y. Liu, *Nano Lett.* **2017**, *17*, 6759.
[24] J. D. Shi, W. Y. Ge, W. X. Gao, M. M. Xu, J. F. Zhu, Y. X. Li, *Adv. Opt. Mater.* **2020**, *8*, 1901516.
[25] L. Qiu, H. Yang, Z. G. Dai, F. X. Sun, J. R. Hao, M. Y. Guan, P. P. Dang, C. J. Yan, J. Lin, G. G. Li, *Inorg. Chem. Front.* **2020**, *7*, 2060.
[26] J. D. Shi, W. Y. Ge, Y. Tian, M. M. Xu, W. X. Gao, Y. T. Wu, *Small* **2021**, *17*, 2006568.
[27] W. H. Wang, M. S. Zhang, F. Deng, Z. M. Wang, Y. Wang, *Appl. Phys. Lett.* **2021**, *119*, 051102.
[28] M. A. Sikandar, W. Ahmad, M. H. Khan, F. Ali, M. Waseem, *Constr. Build. Mater.* **2019**, *228*, 116823.
[29] D. Dorosz, J. Swiderski, A. Zajac, *Eur. Phys. J. Spec. Top.* **2008**, *154*, 51.
[30] M. L. Qin, X. T. Wang, Z. F. Wang, Y. Ma, H. Liu, *Int. J. Appl. Ceram. Technol.* **2018**, *15*, 1047.
[31] J. D. Shi, M. Q. Wang, C. Zhang, J. N. Wang, Y. Zhou, Y. L. Xu, N. V. Gaponenko, *J. Mater. Chem. C* **2023**, *11*, 4742.
[32] J. D. Shi, M. Q. Wang, C. Zhang, J. N. Wang, Y. Zhou, Y. L. Xu, N. V. Gaponenko, *Mater. Today Chem.* **2023**, *29*, 101480.
[33] L. Protesescu, S. Yakunin, M. I. Bodnarchuk, F. Krieg, R. Caputo, C. H. Hendon, R. X. Yang, A. Walsh, M. V. Kovalenko, *Nano Lett.* **2015**, *15*, 3692.
[34] S. M. Suresh, D. Hall, D. Beljonne, Y. Olivier, E. Zysman-Colman, *Adv. Funct. Mater.* **2020**, *30*, 1908677.
[35] X. G. Zhang, Y. M. Huang, M. L. Gong, *Chem. Eng. J.* **2017**, *307*, 291.
[36] B. Conings, J. Drijkoningen, N. Gauquelin, A. Babayigit, J. D'Haen, L. D'Olieslaeger, A. Ethirajan, J. Verbeeck, J. Manca, E. Mosconi, F. De Angelis, H. G. Boyen, *Adv. Energy Mater.* **2015**, *5*, 1500477.
[37] Y. Wei, Z. Y. Cheng, J. Lin, *Chem. Soc. Rev.* **2019**, *48*, 405.
[38] J. D. Shi, M. Q. Wang, H. Wang, C. Zhang, Y. Q. Ji, J. N. Wang, Y. Zhou, A. S. Bhatti, *Nanoscale* **2022**, *14*, 16548.
[39] Y. Q. Ji, M. Q. Wang, Z. Yang, H. W. Qiu, M. A. Padhiar, Y. Zhou, H. Wang, J. L. Dang, N. V. Gaponenko, A. S. Bhatti, *J. Phys. Chem. Lett.* **2021**, *12*, 3786.
[40] J. D. Shi, W. Y. Ge, J. F. Zhu, M. Saruyama, T. Teranishi, *ACS Appl. Nano Mater.* **2020**, *3*, 7563.
[41] H. C. Cho, S. H. Jeong, M. H. Park, Y. H. Kim, C. Wolf, C. L. Lee, J. H. Heo, A. Sadhanala, N. Myoung, S. Yoo, S. H. Im, R. H. Friend, T. W. Lee, *Science* **2015**, *350*, 1222.
[42] D. Shi, V. Adinolfi, R. Comin, M. J. Yuan, E. Alarousu, A. Buin, Y. Chen, S. Hoogland, A. Rothenberger, K. Katsiev, Y. Losovyj, X. Zhang, P. A. Dowben, O. F. Mohammed, E. H. Sargent, O. M. Bakr, *Science* **2015**, *347*, 519.
[43] A. D. Wright, C. Verdi, R. L. Milot, G. E. Eperon, M. A. Perez-Osorio, H. J. Snaith, F. Giustino, M. B. Johnston, L. M. Herz, *Nat. Commun.* **2016**, *7*, 11755.
[44] J. M. Frost, K. T. Butler, F. Brivio, C. H. Hendon, M. van Schilfgaarde, A. Walsh, *Nano Lett.* **2014**, *14*, 2584.
[45] F. Zhang, H. Z. Zhong, C. Chen, X. G. Wu, X. M. Hu, H. L. Huang, J. B. Han, B. S. Zou, Y. P. Dong, *ACS Nano* **2015**, *9*, 4533.
[46] S. Gonzalez-Carrero, R. E. Galian, J. Pérez-Prieto, *J. Mater. Chem. A* **2015**, *3*, 9187.
[47] S. Gonzalez-Carrero, L. Francés-Soriano, M. González-Béjar, S. Agouram, R. E. Galian, J. Pérez-Prieto, *Small* **2016**, *12*, 5245.
[48] S. Q. Huang, Z. C. Li, B. Wang, N. W. Zhu, C. Y. Zhang, L. Kong, Q. Zhang, A. D. Shan, L. Li, *ACS Appl. Mater. Interfaces* **2017**, *9*, 7249.
[49] Z. C. Li, L. Kong, S. Q. Huang, L. Li, *Angew. Chem., Int. Ed.* **2017**, *56*, 8134.